



Utilization of MoS₂ and graphene to enhance the photocatalytic activity of Cu₂O for oxidative C–C bond formation

Zhen Li, Yuxi Pi, Danyun Xu, Yang Li*, Wenchao Peng, Guoliang Zhang, Fengbao Zhang*, Xiaobin Fan*

School of Chemical Engineering and Technology, State Key Laboratory of Chemical Engineering, Collaborative Innovation Center of Chemical Science and Engineering, Tianjin University, Tianjin 300350, China

ARTICLE INFO

Article history:

Received 8 February 2017
Received in revised form 6 April 2017
Accepted 2 May 2017
Available online 3 May 2017

Keywords:

Photocatalyst
Graphene
MoS₂
Cu₂O
Organic synthesis

ABSTRACT

Visible light driven photoredox catalysis has considered as a sustainable and promising strategy for organic synthesis. Here we report a new composite material consisting of cuprous oxide (Cu₂O) nanoparticles grown on layered molybdenum disulfide (MoS₂) and graphene hybrids as a high-performance photocatalyst for C–C bond formation reaction. This composite material shows superior stability and reusability. The enhanced photocatalytic activity of the novel catalyst is attributed to the synergistic effects of MoS₂ and graphene as cocatalysts in the composite, in which graphene serves as an excellent electron transporter, and MoS₂ nanosheets provide a source of active sites. This work would open a promising way to design and fabricate the efficient composite photocatalysts for organic synthesis.

© 2017 Elsevier B.V. All rights reserved.

1. Introduction

As the major part of the sunlight, visible light is considered as a clean, abundant, and sustainable energy resource. So far, visible light photocatalysis has attracted most attention in organic synthesis [1,2]. Notably, carbon–carbon (C–C) bond formation is paramountly important to the organic synthesis chemistry, like pharmaceutical and agrochemical synthesis [3]. In the past decade, many green and sustainable protocols for visible-light-driven C–C bond formation have been developed [4–6]. Currently, Stephenson reported an oxidative C–C bond formation by nitroalkanes and *N*-arylamines under visible light [7]. Since then, several synthetic applications have emerged, and the oxidative C–C bond formation is becoming one of the most exploited photocatalytic transformations [8–11]. On the other hand, for visible-light-driven organic synthesis, fabricating suitable photoredox catalysts, with the ability to absorb the photons in the visible region, is of crucial importance [9]. Nowadays, homogeneous organic dyes [12,13] and transition-metal complexes [6,14,15] are mostly employed in photoredox reactions. However, their high cost, potential toxicity and the difficulty to separate them from the reaction systems hinder the

practical applications of these photocatalysts. The photocatalysts' reuse and recover ability can not only eliminate the contamination of the organic products but also reduce the waste disposal cost in large-scale reactions. Therefore, many efforts have been devoted to heterogeneous photocatalysts in recent years [4,16–19]. Particularly, some semiconductors with suitable band gaps can act as heterogeneous visible-light-driven catalysts in photoredox reactions [20–23].

Cuprous oxide (Cu₂O), a typical p-type semiconductor with direct band gap around 2.0 eV, is considered as a promising photocatalyst in degradation of organic pollutants [24–26], water splitting [27,28] and organic synthesis [9,29]. Besides, considering its unique green characteristics, such as non-toxicity, earth abundance and environmental compatibility, Cu₂O has a great potential to be employed as a photocatalyst in practical applications in chemical industry. Unfortunately, its application is still severely hampered because of the low photocatalytic efficiency caused by fast electron–hole recombination and the poor stability owing to photocorrosion [30,31].

In order to solve such problems, cocatalysts are always introduced in photocatalysts. Recently, graphene, a single layer of graphite, has emerged as a versatile material in the field of material science. Due to its excellent electron conductivity and high specific surface area, it has been used as an efficient cocatalyst to facilitate the charge transfer and electron–hole separation in photocatalysis [32–34]. Besides, molybdenum disulfide (MoS₂) is becoming

* Corresponding authors.

E-mail addresses: liyang1895@tju.edu.cn (Y. Li), fbzhang@tju.edu.cn (F. Zhang), xiabinfan@tju.edu.cn (X. Fan).



another promising photocatalytic cocatalyst. MoS_2 has a two-dimensional layered structure consisting of three stacked atom layers (S–Mo–S) held together in a graphite-like manner by the weak van der Waals force [35,36]. Its unique optical and electronic properties [37] lead to tremendous enhancement in the photore-sponse, photoluminescence quantum yield and charge mobility for MoS_2 -based photocatalysts [38–41]. Moreover, graphene and MoS_2 have been employed as cocatalysts to synergistically enhance activity of photocatalysts for H_2 evolution [42–45] and pollutant disposal [46–48]. Nonetheless, utilizing graphene and MoS_2 as dual cocatalysts in photocatalytic organic synthesis has not been reported to date.

Here we report the preparation of Cu_2O nanoparticles on layered MoS_2 /graphene (MG) hybrids for photocatalytic C–C bond formation reaction. The activity of Cu_2O is remarkably enhanced by the synergistic effect between the components. The catalyst can be also easily recovered and reused with acceptable efficiency for several times.

2. Experimental

2.1. Synthesis of layered MoS_2 /graphene (MG) hybrids

Graphene oxide (GO) was prepared from natural graphite powder by a modified Hummers method. In a typical synthesis of the MoS_2 /graphene (MG) hybrids, 242 mg (1 mmol) of $\text{Na}_2\text{MoO}_4 \cdot 2\text{H}_2\text{O}$, 380 mg (5 mmol) of thiourea and 15 mg of GO were gradually added into 60 mL of deionized (DI) water. The obtained mixture was transferred into a 100 mL Teflon-lined autoclave, and it was held at 210 °C for 24 h [42,46]. After filtration and washing with ethanol and DI water respectively, the black precipitates were completely dried by lyophilization.

2.2. Synthesis of Cu_2O – MoS_2 /graphene (CMG) composite photocatalyst

In a typical preparation process, 170 mg (1 mmol) of $\text{CuCl}_2 \cdot \text{H}_2\text{O}$, 20 mg of sodium dodecyl sulfate (SDS) and a predetermined amount of MG was dispersed in 250 mL DI water via ultrasonication. Subsequently, 80 mg (2 mmol) of NaOH was added into the mixture under magnetic stirring for 30 min. Then, 176 mg (1 mmol) of ascorbic acid was added into the above suspension. After further stirring of 30 min, it was formed a brick red dispersion. The resulting precipitate was collected, washed thoroughly with ethanol and DI water respectively, and dried under vacuum. The bare Cu_2O nanoparticles were prepared following the same method without the addition of the MoS_2 /graphene hybrids.

2.3. Photocatalytic ability toward C–C bond formation reaction

20.9 mg (0.1 mmol) *N*-aryl-tetrahydroisoquinoline, 2.0 mg CMG and 1 mL nitromethane were added in a Schlenk tube and mixed by ultrasonication for 2 min. In an oxygen atmosphere, the mixture was stirred under irradiation using a 24 W compact fluorescent

bulb. After 8 h, the catalyst was separated by filtration, and the filtrate was analyzed by gas chromatography (GC). The generated H_2O_2 in the system was measured by a colorimetric method with copper (II) ions and DMP at 454 nm [49].

2.4. Photoelectrochemical measurements

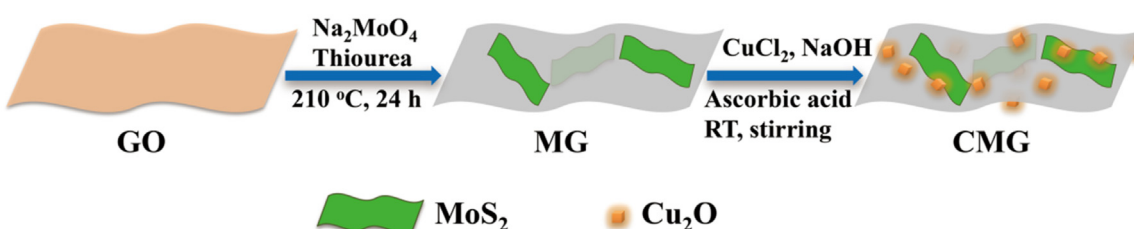
Photocurrent was measured on an electrochemical analyzer (CHI660E Instruments) in a standard three-electrode system. The prepared samples were used as the working electrodes with an active area of 1.0 cm^2 . A Pt wire was used as the counter electrode, and Ag/AgCl (saturated KCl) was the reference electrode. A 300 W Xe lamp (Perfectlight Microsolar300) equipped with an AM1.5 filter was used as a light source. 0.01 M Na_2SO_4 aqueous solution was employed as the electrolyte. The working electrodes were prepared as follows: 0.25 g of the sample was mixed 0.5 mL ethanol to make a slurry. Then, the slurry was coated onto an F-doped SnO_2 -coated glass (FTO glass) electrode. The electrodes were dried in the dark at room temperature.

2.5. Characterization

The samples were characterized by scanning electron microscopy (SEM; Hitachi S4800), transmission electron microscopy (TEM; JEM-2100F), X-ray photoelectron spectroscopy (XPS; PerkinElmer, PHI1600 spectrometer), X-ray diffraction (XRD; AXS D8-Focus), Raman spectroscopy (Renishaw, inVia reflex), UV-vis diffuse reflectance spectroscopy (UV-DRS; Thermo Scientific Evolution 300) and photoluminescence (PL) spectroscopy (Jobin Yvon, Fluorolog 3-21). Electron spin resonance (ESR) spectra were recorded at room temperature using a Bruker EMXplus spectrometer. The catalytic reactions were monitored by a gas chromatography (GC; Agilent 6890N GC-FID system).

3. Results and discussion

The Cu_2O – MoS_2 /graphene (CMG) composite photocatalysts were prepared by a facile two-step process as illustrated in Scheme 1. Firstly, the layered MoS_2 /graphene (MG) was fabricated by the hydrothermal reaction. During this process, the graphene-like MoS_2 nanosheets emerged on the graphene sheets which were reduced from GO simultaneously (Fig. S1). Subsequently, CMG composites were generated by in-situ growth of Cu_2O nanoparticles on MoS_2 /graphene (MG) hybrids. The scanning electron microscopy images (SEM) and transmission electron microscopy (TEM) show that the layered MG is provided as a novel support for Cu_2O nanoparticles loading (Fig. 1a, b and S2). The high-resolution TEM (HRTEM) image (Fig. 1c) verifies that the Cu_2O nanoparticles are adhered to the MG hybrids. The lattice fringes with a d spacing of 0.21 nm can be assigned to the (200) lattice planes of Cu_2O . It is worth noting that the dark lattice fringes spaced by 0.62 nm is corresponded to the (002) van der Waals planes of MoS_2 [50]. Additionally, high-angle annular dark field scanning transmission electron microscopy (HAADF-STEM) and corresponding quantita-



Scheme 1. Illustration of the Cu_2O – MoS_2 /graphene (CMG) photocatalyst synthesis.

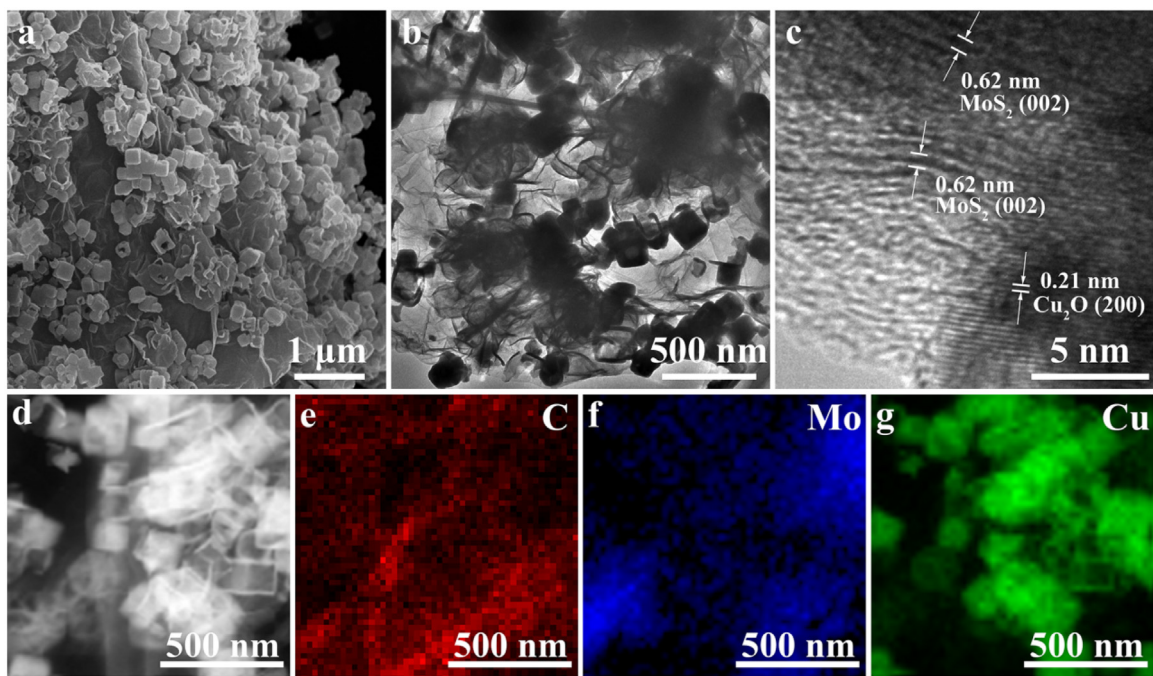


Fig. 1. (a) SEM, (b) TEM and (c) HRTEM images of $\text{Cu}_2\text{O}-\text{MoS}_2$ /graphene (CMG) composite. (d) HAADF-STEM image of CMG and corresponding quantitative EDS mapping of (e) C, (f) Mo and (g) Cu.

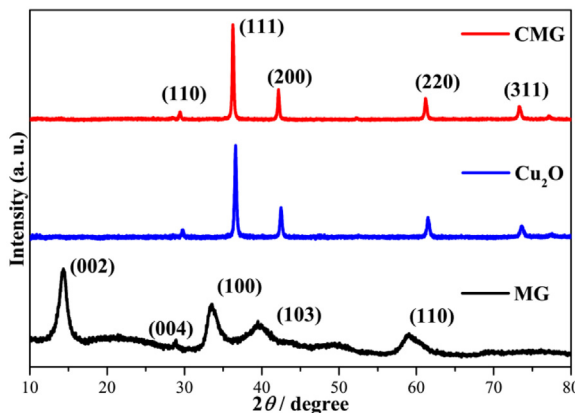


Fig. 2. XRD patterns of MoS_2 /graphene (MG) hybrids, Cu_2O and $\text{Cu}_2\text{O}-\text{MoS}_2$ /graphene (CMG) composite.

ative energy dispersive X-ray spectroscopy (EDS) mapping indicate the distributions of elements C, Mo, and Cu on the surface of CMG, demonstrating the successful growths of Cu_2O and MoS_2 on graphene (Fig. 1d–g). Moreover, pure Cu_2O , MG and CMG composite were characterized by powder XRD (Fig. 2). The MG shows five obvious peaks at 14.4° , 28.8° , 33.4° , 39.5° and 58.8° which are corresponded respectively to the (002), (004), (100), (103) and (110) planes of MoS_2 [42]. Besides, characteristic peaks at around 29.5° , 36.4° , 42.3° , 61.3° and 73.5° are assigned to (110), (111), (200), (220) and (311) planes of Cu_2O , respectively [25]. Notably, those peaks can be found in both CMG and pure Cu_2O . Furthermore, no characteristic diffraction peaks for MoS_2 and carbon species are observed because of the low amount and relatively low diffraction intensity of MoS_2 and graphene in the composite [46,48]. Graphene and MoS_2 are expected to form a desirable heterostructure, which may facilitate the vectorial transfer of photogenerated electrons from Cu_2O to graphene and/or MoS_2 , thus enhancing the charge separation and photocatalytic efficiency.

In order to characterize the chemical composition of as-prepared $\text{Cu}_2\text{O}-\text{MoS}_2$ /graphene photocatalyst, X-ray photoelectron spectroscopy (XPS) is employed to determine the exact surface state. Fig. 3a displays the XPS spectrum of Cu 2p, which contains $\text{Cu} 2\text{p}_{3/2}$ at 932.6 eV and $\text{Cu} 2\text{p}_{1/2}$ at 952.5 eV , indicating the existence of cuprous state [51]. Additionally, the XPS in the Mo 3d range of CMG exhibits a peak at 226.7 eV corresponding to the S 2s of MoS_2 (Fig. 3b). Meanwhile, two doublets composed of Mo 3d_{3/2} and Mo 3d_{5/2} are located at 232.4 eV and 229.2 eV respectively, demonstrating that Mo element exists in the chemical formation of Mo^{4+} (Fig. 3b) [52,53]. Similarly, S 2p spectrum can be fitted into two peaks at 163.3 eV and 162.2 eV , as revealed in Fig. 3c, which are separately belonging to S 2p_{1/2} and S 2p_{3/2}, suggesting that S is in the form of S^{2-} [54]. The results of XPS spectra of Mo 3d and S 2p indicate the existence of MoS_2 in the composite. Regarding the C 1s spectrum in Fig. 3d, the peak at 284.7 eV is assigned to the sp^2 bonded carbon (C–C) present in graphitic domains. Note that, compared with GO (Fig. S3), peaks of carboxyl ($\text{O}=\text{C}–\text{O}$) at 288.7 eV , hydroxyl ($\text{C}–\text{OH}$) and epoxy ($\text{O}–\text{C}–\text{O}$) groups at 286.5 eV decrease in the composite, verifying the reduction of GO during the preparation process [45].

Raman spectroscopy is one of the prominent tools for characterizing the structural bonding nature, crystallinity and associated defect levels in two-dimensional nanostructures such as graphene, layered TMDs, and nanocomposites. As shown in Fig. 4, compared with GO, another two major peaks appear in Raman spectrum of MG. The peak of E_{2g}^1 mode at around 380 cm^{-1} is associated with the vibrations (in-plane) of two sulfur atoms with the molybdenum atom, while the A_{1g} mode near 400 cm^{-1} corresponding to the vibrations (out-of-plane) of sulfur atoms in opposite directions [53,55]. Moreover, D band (at around 1300 cm^{-1}) and G band (at around 1600 cm^{-1}) of graphene are observed in all samples. The former corresponds to the surface defects of the graphene, as the latter to the formation of sp^2 -bonded crystalline carbon in graphene [56]. Notably, MG has a lower $\text{I}_\text{D}/\text{I}_\text{G}$ intensity ratio (1.04) than GO (1.56) with the G band shifting from 1602 to 1589 cm^{-1} , indicating an increase in the proportion of sp^2 conjugated carbon atoms.

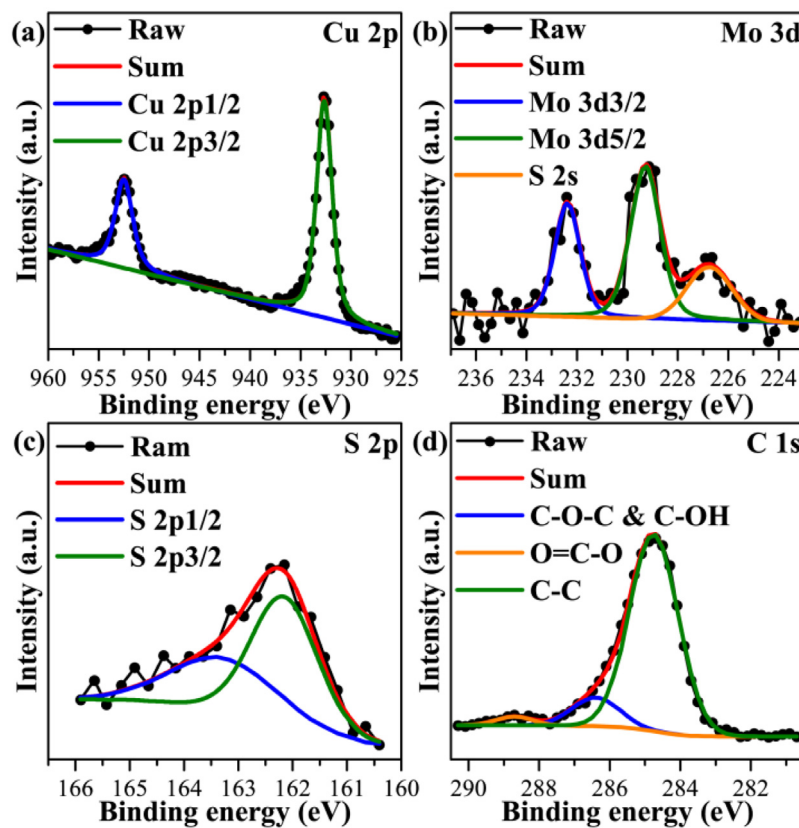


Fig. 3. (a) Cu 1p, (b) Mo 3d, (c) S 2p and (d) C 1s XPS spectra of Cu₂O–MoS₂/graphene (CMG).

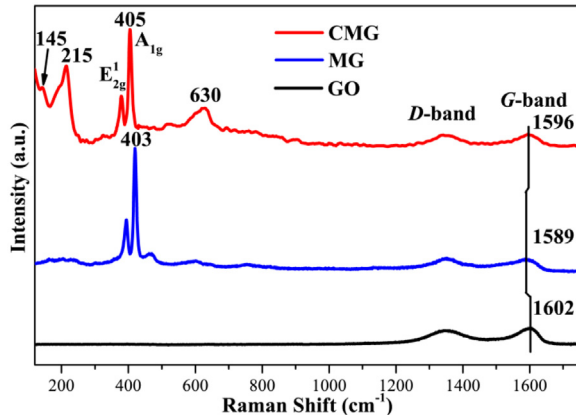


Fig. 4. Raman spectra of GO, MG and CMG.

Additionally, the sp^3 hybridized carbon atoms are converted to sp^2 conjugation during the hydrothermal treatment process. The emerged characteristic peaks of MoS₂ and the changes of I_D/I_G radio and G band indicated that GO is reduced, simultaneously as MoS₂ nanosheets are formed. After loading of Cu₂O, three vibrational fingerprints of Cu₂O appear at 145, 630 and 215 cm⁻¹, corresponding to two infrared-allowed modes and a second-order overtone respectively [57]. Moreover, it is worth noting that the A_{1g} band in CMG upshifts to 405 cm⁻¹. In MoS₂-based composites, mismatch of the lattice spacing between MoS₂ and other materials may change the local strain on the surface of MoS₂ nanosheets [58]. Meanwhile, A_{1g} mode of MoS₂ is highly sensitive to tensile or compressive strain, and variation of the local strain may lead to shifts of A_{1g} band in Ramam spectra [59,60]. Hence, it is supposed that introducing of Cu₂O may change the local strain on the surface of MoS₂

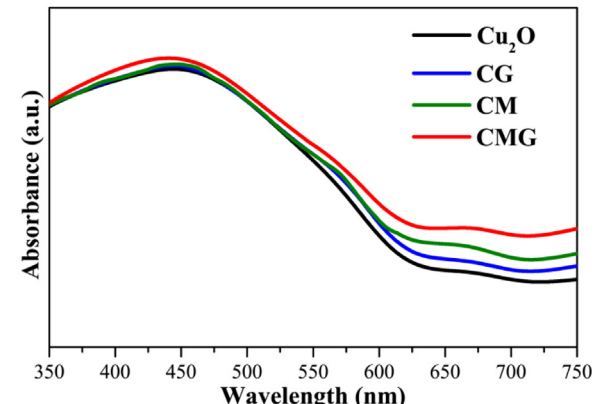


Fig. 5. UV–vis diffuse reflectance spectra of Cu₂O, CG, CM and CMG.

nanosheets, resulting in the A_{1g} band upshifting in CMG. Additionally, the G band in CMG upshifts to 1596 cm⁻¹, presumably due to the change in the skeletal structure of graphene caused by closely integrated with Cu₂O [61–63].

The UV-vis diffuse reflectance spectra of Cu₂O, Cu₂O/graphene (CG), Cu₂O/MoS₂ (CM) and Cu₂O–MoS₂/graphene (CMG) are compared in Fig. 5. After combined with graphene, MoS₂, or MoS₂/graphene hybrids, the enhanced absorption in the visible region is observed compared to pure Cu₂O, which can be attributed to the light absorption of cocatalysts. Notably, the absorption edge of CMG redshifts to longer wavelength than other samples, indicating that the MoS₂/graphene incorporation can greatly extend the light absorption of the photocatalysts towards the visible light region, allowing a more efficient utilization of solar energy for the photocatalytic applications [43].

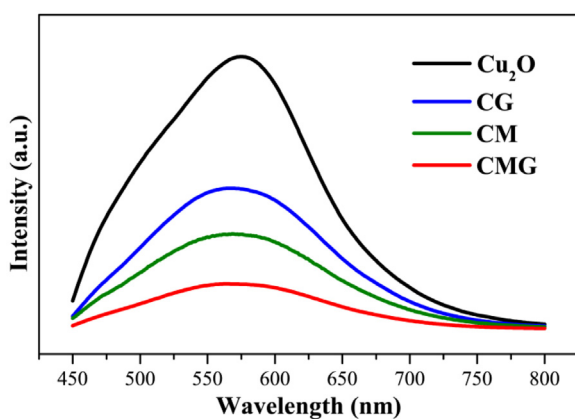
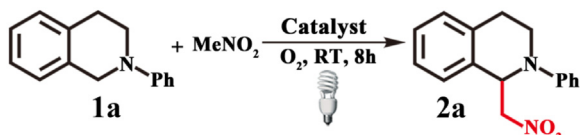


Fig. 6. photoluminescence (PL) spectra of Cu_2O , CG, CM and CMG.



Scheme 2. Oxidative coupling reaction of *N*-aryl-tetrahydroisoquinoline with nitromethane.

Table 1
Oxidative coupling reaction of *N*-aryl-tetrahydroisoquinoline with nitromethane^a.

entry	catalyst	yield [%] ^b	selectivity [%]
1	blank	2	11
2	CMG ^c	3	13
3	graphene	2	12
4	MoS_2	5	24
5	MG	10	78
6	Cu_2O	60	72
7	CG	63	75
8	CM	64	76
9	CMG	79	82
10	Eosin Y	26	41
11	TiO_2	15	32

^a Standard conditions: 1a (0.1 mmol) and catalyst were added in nitromethane (1 mL). The reaction was run in a Schlenk tube with an attached oxygen balloon and irradiated with a 24 W compact fluorescent bulb for 8 h.

^b Calibrated yields determined by GC.

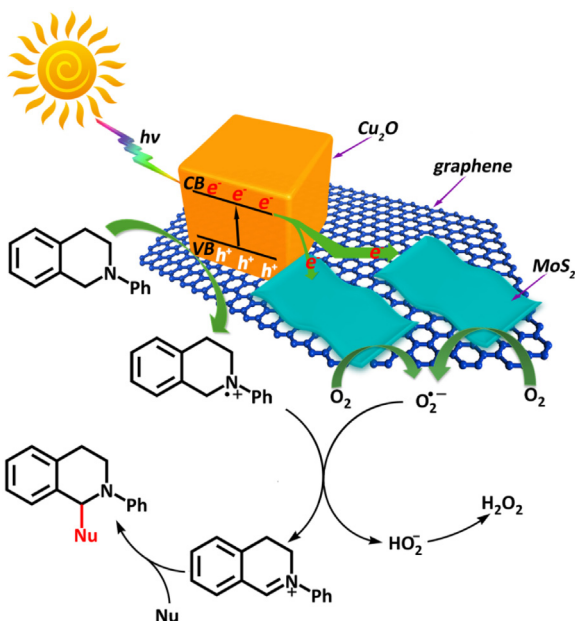
^c The reaction was carried out in the dark.

The photoluminescence (PL) spectra have been widely used to reveal the transfer, migration and recombination processes of the photogenerated electron–hole pairs in materials. As shown in Fig. 6, Cu_2O has the highest PL emission intensity, and the PL intensity of CMG is much lower than those of CM and CG. It is indicated that both MoS_2 and graphene can promote the efficient charge separation, prolong the life time of the carriers and hamper the recombination of photogenerated electron–hole pairs. Meanwhile, the most effective suppression of undesirable energy-wasting and charge recombination process may contribute to the lowest PL intensity of CMG, which in further improving the photocatalytic activity [46,48].

The catalytic activities of investigated catalyst materials were evaluated by photocatalytic oxidative C–C bond formation reaction using *N*-aryl-tetrahydroisoquinoline (1a) as the amine substrate and nitromethane as the solvent (Scheme 2). Several control experiments were also performed for comparison purposes. The results were summarized in Table 1. Without catalyst (entry 1, Table 1) or light (entry 2, Table 1), only limited yields of 2% and 3% were observed for the desired product (2a), respectively. As comparisons, graphene (entry 3, Table 1) hardly catalyzed this reaction

(yield of 2% and selectivity of 12%), and MoS_2 (entry 4, Table 1) showed a low intrinsic photocatalytic activity (yield of 5% and selectivity of 24%). However, bare MG presented a modestly higher yield of 10% and a superior selectivity of 78% (entry 5, Table 1). It may presumably be attributed to the unique electronic property and two-dimensional structure of graphene, which could facilitate the electron transport in photocatalysis and the mass transmission of the reactants/products, respectively. Meanwhile, pure Cu_2O showed a mediocre photocatalytic performance (with 60% yield and 72% selectivity) in this reaction (entry 6, Table 1), probably due to the rapid recombination of conduction band (CB) electrons and valence band (VB) holes. Combined with graphene or MoS_2 alone, Cu_2O had a higher photocatalytic performance than pure Cu_2O (entry 7 and 8, Table 1). Delightedly, the introduction of MG remarkably enhanced the photocatalytic activity of Cu_2O nanoparticles, with a yield of 79% and a selectivity of 82% for desired products (entry 9, Table 1). The improved activity could be due to the synergistic effect of graphene and MoS_2 on Cu_2O . In addition, two typical photocatalysts, Eosin Y and commercial TiO_2 were used to catalyze the reaction with the same conditions. However, compared with CMG, both of them showed inferior photocatalytic activity (entry 10 and 11, Table 1). Eosin Y, as a homogenous photocatalyst, may be hampered by its intrinsic photocatalytic activity and the difficulty to recovery [16]. Meanwhile, TiO_2 , as a heterogeneous photocatalyst, may not efficiently absorb visible light due to its relatively wide bandgap, resulting in its limited photocatalytic performance [42]. Besides, the photocatalytic reaction rates of pure Cu_2O , CG, CM and CMG were explored. As shown in Fig. S4, this photocatalytic C–C bond formation was approximately fitted as a zero order reaction, which meant that the concentration of the reagents in the system might not obviously affect the reaction rate [9]. Interestingly, CMG had the highest reaction rate among all them, indicating that MoS_2 and graphene synergistically facilitated the photocatalytic activity of Cu_2O . The stability and reusability of the CMG catalyst were tested by repeated experiments. Notably, CMG showed excellent stability upon reuse. It could maintain its catalytic performances for at least successive six cycles without obvious decline in its activity (Fig. S5). Moreover, compared with fresh catalysts, the XRD plot and SEM image of reused catalysts did not show obvious change after experiments, suggesting a good structural stability of CMG (Fig. S6 and S7).

To investigate the mechanism involved, controlled experiments with addition of different radical scavengers in the photocatalytic oxidative C–C bond formation over bare Cu_2O , CG, CM and CMG were carried out. Considering that superoxide radicals and/or hydroxyl radicals might be involved in the reactions, benzoquinone (BQ) was employed as the scavenger for superoxide radicals, and *tert*-butyl alcohol (TBA) was used for hydroxyl radicals. As shown in Fig. S8, with BQ, the yields of desired products remarkably decreased. Nevertheless, TBA barely influenced on the photocatalytic activity of the photocatalysts. Obviously, superoxide radicals might play a crucial role in the reactions. Moreover, electron spin resonance (ESR) spectroscopy was used to detect the radicals generated by bare Cu_2O , CG, CM and CMG, with 5,5-dimethyl-1-pyrroline-N-oxide (DMPO) added as a probe (Fig. S9). The $\text{DMPO}-\text{O}_2^{\bullet-}$ species were detected in all the samples, whereas no such signals were detected in the dark, indicating that $\text{O}_2^{\bullet-}$ was generated under irradiation [64]. To our delight, CMG shows the superior intensity of $\text{DMPO}-\text{O}_2^{\bullet-}$ species, demonstrating the highest concentration of superoxide radicals in the CMG system [65]. Considering these, the mechanism proposed for the superior photocatalytic activity of CMG is illustrated in Scheme 3. Under visible light illumination, the valence band (VB) electrons of Cu_2O nanoparticles are excited to conduction band (CB), creating holes in the VB simultaneously, and then the CB electrons of Cu_2O inject into the graphene sheets. Due to the high electri-



Scheme 3. Proposed mechanism for oxidative C–C bond formation reaction photocatalyzed by CMG under visible light.

cal conductivity of graphene, the mobility of these electrons on the graphene is extremely high, which functions as an excellent electron transporter to lengthen the life time of the charge carriers [32]. Meanwhile, the MoS₂ nanosheets can accept electrons (either directly from Cu₂O or through the graphene electron transfer mediator) [42,45,47,50]. Transient photocurrent experiments (Fig. S10) further demonstrated an obviously enhancement in the charge transport from Cu₂O to graphene and/or MoS₂ and then to the surface of the working electrode, additionally confirming the suggested transfer process of electrons [42]. Additionally, in previous studies, nanoscale MoS₂ has been used to facilitate the formation of superoxide radical anions (O₂[•]) during the photocatalysis

as a cocatalyst [46], due to its ability to activate O₂ [66]. Generally, the catalytic activity of MoS₂ is closely related to its active edge sites [67,68]. The Mo atoms on the edges of MoS₂ may serve as a preferred location for the absorption of oxygen and superoxide radical anions (O₂[•]) can be formed with charge transfer [68,69]. On the other hand, the VB hole, which is generated under light irradiation, is able to abstract an electron from the tertiary amine via a single electron transfer (SET) process, presumably [9]. The tertiary amine radical cation donates one hydrogen atom to the superoxide radical anion and results in the formation of an iminium ion. The iminium ion can be trapped by nucleophiles to release the final product [70]. Moreover, the large surface area of MG can facilitate the absorption of the reactants [42,46]. Meanwhile, the graphene can improve the rapid photogenerated electron transfer and the MoS₂ may activate O₂, which provide more reaction centers in the composite, as reactions may not just occur on Cu₂O [32,71]. Therefore, as dual cocatalysts, graphene and MoS₂ synergistically enhance the photocatalytic performance of Cu₂O.

The graphene content in cocatalyst was optimized for the synthesis of the CMG based on the C–C bond formation reaction results. As shown in Fig. S11, while the weight percentage of the MoS₂/graphene (MG) hybrids in the composites was fixed at 7%, the graphene content in the hybrids varied. The addition of the graphene content in the layered MG hybrids improved the photo-activity of Cu₂O. Containing MoS₂/9.7graphene hybrids (9.7 means that the weight percentage of MoS₂ in MG is 9.7%), the photocatalyst showed the best photocatalytic performance. Then the photo-activity gradually reduced with the further increase of the graphene content in the cocatalyst. On this account, the MoS₂/9.7graphene hybrids were determined to compose the cocatalyst. The amount of cocatalyst in CMG was also optimized. Fig. S11 indicated that the photocatalytic activity of CMG composite increased with increasing amount of cocatalyst and reached a maximum yield and selectivity for the composite containing 7% hybrid cocatalyst. A further increase in the amount of MG led to a reduction of the activity. Accordingly, it is supposed that excess MoS₂ and graphene may induce a “shielding effect”. Due to this effect, the incident light is shielded from irradiating into the inside of the catalysts [42,44]. Additionally, the active sites of the surface of Cu₂O

Table 2
Oxidative coupling reaction of *N*-aryl-tetrahydroisoquinoline with different substrates by CMG^a.

entry	substrate	product	Yield[%] ^b	Selectivity[%]
1	MeNO ₂		79	82
2	EtNO ₂		70	71
3			60	80
4			61	73
5			55	72
6			52	64

^a Standard conditions: 1a (0.1 mmol) and catalyst were added in nitromethane (1 mL). The reaction was run in a Schlenk tube with an attached oxygen balloon and irradiated with a 24 W compact fluorescent bulb for 8 h.

^b Calibrated yields determined by GC.

may be covered by MG, hindering the contact of reactant and active sites [44,46].

The catalytic performance of CMG in the oxidative coupling reactions of *N*-aryl-tetrahydroisoquinolines with different substrates were also investigated, and the results are summarized in Table 2. Compared with bare Cu₂O nanoparticles (Table S2), CMG shows superior photocatalytic abilities, indicating the enhance effect of MoS₂/graphene in photocatalytic oxidative C–C bond formation reaction.

4. Conclusions

In summary, we successfully loaded Cu₂O nanoparticles on layered MoS₂/graphene (MG) hybrids to synthesize a novel photocatalytic composite through a two-step method. Compared with bare Cu₂O, the Cu₂O–MoS₂/graphene (CMG) composite catalyst exhibited a remarkably superior photocatalytic performance in C–C bond formation reaction. CMG containing 7% MG hybrids, with 90.3% MoS₂ and 9.7% graphene, the composite had the most effective activity, with a yield of 79% and selectivity of 82% for desired products. It was shown that graphene and MoS₂ could enhance the photocatalytic performance of Cu₂O. The layered MoS₂/graphene could facilitate interfacial charge transfer efficiently suppressing charge recombination. Moreover, it may provide not only more numerous active sites allowed for the activation of O₂ for the photocatalysis, but also added photocatalytic reaction centers. The Cu₂O–MoS₂/graphene composite also had good stability and reusability. Notably, this is the first to use MoS₂ and graphene as cocatalysts to synergistically enhance the photocatalyst in organic synthesis.

Acknowledgments

This study is supported by the National Natural Science Funds (No. 21676198, No. 21506157), the Program of Introducing Talents of Discipline to Universities (No. B06006), the Doctoral Program of Higher Education of China (No. 20130032120017) and the Natural Science Foundation of Tianjin (No. 14JCQNJC05800).

Appendix A. Supplementary data

Supplementary data associated with this article can be found, in the online version, at <http://dx.doi.org/10.1016/j.apcatb.2017.05.010>.

References

- [1] K.L. Skubi, T.R. Blum, T.P. Yoon, *Chem. Rev.* 116 (2016) 10035–10074.
- [2] Q.M. Kainz, C.D. Matier, A. Bartoszewicz, S.L. Zultanski, J.C. Peters, G.C. Fu, *Science* 351 (2016) 681–684.
- [3] D.A. Colby, R.G. Bergman, J.A. Ellman, *Chem. Rev.* 110 (2010) 624–655.
- [4] P. Wu, C. He, J. Wang, X. Peng, X. Li, Y. An, C. Duan, *J. Am. Chem. Soc.* 134 (2012) 14991–14999.
- [5] J.D. Cuthbertson, D.W. MacMillan, *Nature* 519 (2015) 74–77.
- [6] K. Mori, M. Kawashima, H. Yamashita, *Chem. Commun.* 50 (2014) 14501–14503.
- [7] A.G. Condie, J.C. Gonzalez-Gomez, C.R. Stephenson, *J. Am. Chem. Soc.* 132 (2010) 1464–1465.
- [8] H. Bartling, A. Eisenhofer, B. König, R.M. Gschwind, *J. Am. Chem. Soc.* 138 (2016) 11860–11871.
- [9] J. Wang, J. Ma, X. Li, Y. Li, G. Zhang, F. Zhang, X. Fan, *Chem. Commun.* 50 (2014) 14237–14240.
- [10] D.P. Hari, B. Konig, *Org. Lett.* 13 (2011) 3852–3855.
- [11] M. Rueping, J. Zoller, D.C. Fabry, K. Poscharny, R.M. Koenigs, T.E. Weirich, J. Mayer, *Chem. Eur. J.* 18 (2012) 3478–3481.
- [12] J. Davies, T.D. Svejstrup, D. Fernandez Reina, N.S. Sheikh, D. Leonori, *J. Am. Chem. Soc.* 138 (2016) 8092–8095.
- [13] S.P. Pitre, C.D. McTiernan, J.C. Scaiano, *Acc. Chem. Res.* 49 (2016) 1320–1330.
- [14] C.K. Prier, D.A. Rankic, D.W. MacMillan, *Chem. Rev.* 113 (2013) 5322–5363.
- [15] E.B. Corcoran, M.T. Pirnot, S. Lin, S.D. Dreher, D.A. DiRocco, I.W. Davies, S.L. Buchwald, D.W. MacMillan, *Science* 353 (2016) 279–283.
- [16] Z. Li, W. Zhang, Q. Zhao, H. Gu, Y. Li, G. Zhang, F. Zhang, X. Fan, *ACS Sustain. Chem. Eng.* 3 (2015) 468–474.
- [17] S. Wang, X. Wang, *Small* 11 (2015) 3097–3112.
- [18] X. Qian, K. Fuku, Y. Kuwahara, T. Kamegawa, K. Mori, H. Yamashita, *ChemSusChem* 7 (2014) 1528–1536.
- [19] K. Mori, H. Yamashita, *Chem. Eur. J.* 22 (2016) 11122–11137.
- [20] M. Cherevatskaya, M. Neumann, S. Fuldrer, C. Harlander, S. Kummel, S. Dankesreiter, A. Pfitzner, K. Zeitler, B. Konig, *Angew. Chem. Int. Ed.* 51 (2012) 4062–4066.
- [21] T. Hisatomi, J. Kubota, K. Domen, *Chem. Soc. Rev.* 43 (2014) 7520–7535.
- [22] K. Li, B. Peng, T. Peng, *ACS Catal.* 6 (2016) 7485–7527.
- [23] T. Kamegawa, S. Matsuura, H. Seto, H. Yamashita, *Angew. Chem. Int. Ed.* 52 (2013) 916–919.
- [24] C.H. Kuo, Y.C. Yang, S. Gwo, M.H. Huang, *J. Am. Chem. Soc.* 133 (2011) 1052–1057.
- [25] W.C. Huang, L.M. Lyu, Y.C. Yang, M.H. Huang, *J. Am. Chem. Soc.* 134 (2012) 1261–1267.
- [26] J. Li, S.K. Cushing, J. Bright, F. Meng, T.R. Senty, P. Zheng, A.D. Bristow, N. Wu, *ACS Catal.* 3 (2013) 47–51.
- [27] Y. Liu, B. Zhang, L. Luo, X. Chen, Z. Wang, E. Wu, D. Su, W. Huang, *Angew. Chem. Int. Ed.* 54 (2015) 15260–15265.
- [28] Z. Lin, J. Xiao, L. Li, P. Liu, C. Wang, G. Yang, *Adv. Energy Mater.* 6 (2016) 1501865.
- [29] K. Sharma, M. Kumar, V. Bhalla, *Chem. Commun.* 51 (2015) 12529–12532.
- [30] A. Paracchino, N. Mathews, T. Hisatomi, M. Stefik, S.D. Tilley, M. Grätzel, *Energy Environ. Sci.* 5 (2012) 8673–8681.
- [31] Z. Zhang, R. Dua, L. Zhang, H. Zhu, H. Zhang, P. Wang, *ACS Nano* 7 (2013) 1709–1717.
- [32] P.D. Tran, S.K. Batabyal, S.S. Pramana, J. Barber, L.H. Wong, S.C. Loo, *Nanoscale* 4 (2012) 3875–3878.
- [33] Q. Xiang, J. Yu, M. Jaroniec, *Chem. Soc. Rev.* 41 (2012) 782–796.
- [34] X. Fan, G. Zhang, F. Zhang, *Chem. Soc. Rev.* 44 (2015) 3023–3035.
- [35] T.F. Jaramillo, K.P. Jorgensen, J. Bonde, J.H. Nielsen, S. Horch, I. Chorkendorff, *Science* 317 (2007) 100–102.
- [36] X. Fan, P. Xu, Y.C. Li, D. Zhou, Y. Sun, M.A. Nguyen, M. Terrones, T.E. Mallouk, *J. Am. Chem. Soc.* 138 (2016) 5143–5149.
- [37] Q.H. Wang, K. Kalantar-Zadeh, A. Kis, J.N. Coleman, M.S. Strano, *Nat. Nanotechnol.* 7 (2012) 699–712.
- [38] F. Meng, J. Li, S.K. Cushing, M. Zhi, N. Wu, *J. Am. Chem. Soc.* 135 (2013) 10286–10289.
- [39] N. Tian, Z. Li, D. Xu, Y. Li, W. Peng, G. Zhang, F. Zhang, X. Fan, *Ind. Eng. Chem. Res.* 55 (2016) 8726–8732.
- [40] K. Chang, X. Hai, J. Ye, *Adv. Energy Mater.* 6 (2016) 1502555.
- [41] Y.-J. Yuan, Z.-J. Ye, H.-W. Lu, B. Hu, Y.-H. Li, D.-Q. Chen, J.-S. Zhong, Z.-T. Yu, Z.-G. Zou, *ACS Catal.* 6 (2016) 532–541.
- [42] Q. Xiang, J. Yu, M. Jaroniec, *J. Am. Chem. Soc.* 134 (2012) 6575–6578.
- [43] K. Chang, Z. Mei, T. Wang, Q. Kang, S. Ouyang, J. Ye, *ACS Nano* 8 (2014) 7078–7087.
- [44] B. Zhu, B. Lin, Y. Zhou, P. Sun, Q. Yao, Y. Chen, B. Gao, *J. Mater. Chem. A* 2 (2014) 3819–3827.
- [45] Y.-J. Yuan, J.-R. Tu, Z.-J. Ye, D.-Q. Chen, B. Hu, Y.-W. Huang, T.-T. Chen, D.-P. Cao, Z.-T. Yu, Z.-G. Zou, *Appl. Catal. B* 188 (2016) 13–22.
- [46] W.C. Peng, X. Wang, X.Y. Li, *Nanoscale* 6 (2014) 8311–8317.
- [47] W.C. Peng, Y. Chen, X.Y. Li, J. Hazard. Mater. 309 (2016) 173–179.
- [48] C. Zhang, G. Chen, C. Li, J. Sun, C. Lv, S. Fan, W. Xing, *ACS Sustain. Chem. Eng.* 4 (2016) 5936–5942.
- [49] X. Zeng, Z. Wang, N. Meng, D.T. McCarthy, A. Deletic, J.-h. Pan, X. Zhang, *Appl. Catal. B* 202 (2017) 33–41.
- [50] Y.-F. Zhao, Z.-Y. Yang, Y.-X. Zhang, L. Jing, X. Guo, Z. Ke, P. Hu, G. Wang, Y.-M. Yan, K.-N. Sun, *J. Phys. Chem. C* 118 (2014) 14238–14245.
- [51] Z. Ai, L. Zhang, S. Lee, W. Ho, *J. Phys. Chem. C* 113 (2009) 20896–20902.
- [52] V.O. Koroteev, L.G. Bulusheva, I.P. Asanov, E.V. Shlyakhova, D.V. Vyalikh, A.V. Okotrub, *J. Phys. Chem. C* 115 (2011) 21199–21204.
- [53] X. Fan, P. Xu, D. Zhou, Y. Sun, Y.C. Li, M.A. Nguyen, M. Terrones, T.E. Mallouk, *Nano Lett.* 15 (2015) 5956–5960.
- [54] D. Merki, S. Fierro, H. Vrubel, X. Hu, *Chem. Sci.* 2 (2011) 1262–1267.
- [55] C. Lee, H. Yan, L.E. Brus, T.F. Heinz, J. Hone, S. Ryu, *ACS Nano* 4 (2010) 2695–2700.
- [56] A.C. Ferrari, J.C. Meyer, V. Scardaci, C. Casiraghi, M. Lazzeri, F. Mauri, S. Piscanec, D. Jiang, K.S. Novoselov, S. Roth, A.K. Geim, *Phys. Rev. Lett.* 97 (2006) 187401.
- [57] D. Powell, A. Compaan, J.R. Macdonald, R.A. Forman, *Phys. Rev. B* 12 (1975) 20–25.
- [58] L. Oakes, R. Carter, T. Hanken, A.P. Cohn, K. Share, B. Schmidt, C.L. Pint, *Nat. Commun.* 7 (2016) 11796.
- [59] Y.Y. Hui, X. Liu, W. Jie, N.Y. Chan, J. Hao, Y.T. Hsu, L.J. Li, W. Guo, S.P. Lau, *ACS Nano* 7 (2013) 7126–7131.
- [60] M.Y. Li, Y. Shi, C.C. Cheng, L.S. Lu, Y.C. Lin, H.L. Tang, M.L. Tsai, C.W. Chu, K.H. Wei, J.H. He, W.H. Chang, K. Suenaga, L.J. Li, *Science* 349 (2015) 524–528.
- [61] H. Wang, Y. Liang, L. Liu, J. Hu, W. Cui, *Appl. Surf. Sci.* 392 (2017) 51–60.
- [62] T. Wang, C. Li, J. Ji, Y. Wei, P. Zhang, S. Wang, X. Fan, J. Gong, *ACS Sustain. Chem. Eng.* 2 (2014) 2253–2258.
- [63] Y. Sang, Z. Zhao, J. Tian, P. Hao, H. Jiang, H. Liu, J.P. Claverie, *Small* 10 (2014) 3775–3782.
- [64] Q. Liu, Y.N. Li, H.H. Zhang, B. Chen, C.H. Tung, L.Z. Wu, *Chem. Eur. J.* 18 (2012) 620–627.

[65] F. Su, S.C. Mathew, G. Lipner, X. Fu, M. Antonietti, S. Blechert, X. Wang, *J. Am. Chem. Soc.* 132 (2010) 16299–16301.

[66] Q. Gao, C. Giordano, M. Antonietti, *Angew. Chem. Int. Ed.* 51 (2012) 11910–11914.

[67] K. Zhao, W. Gu, L. Zhao, C. Zhang, W. Peng, Y. Xian, *Electrochim. Acta* 169 (2015) 142–149.

[68] L. Hao, J. Yu, X. Xu, L. Yang, Z. Xing, Y. Dai, Y. Sun, J. Zou, *J. Power Sour.* 339 (2017) 68–79.

[69] S.J. Rowley-Neale, J.M. Fearn, D.A. Brownson, G.C. Smith, X. Ji, C.E. Banks, *Nanoscale* 8 (2016) 14767–14777.

[70] Y. Pan, C.W. Kee, L. Chen, C.-H. Tan, *Green Chem.* 13 (2011) 2682–2685.

[71] M. Liu, F. Li, Z. Sun, L. Ma, L. Xu, Y. Wang, *Chem. Commun.* 50 (2014) 11004–11007.